IEEE Access
Multidisciplinary | Rapid Review | Open Access Journal

Received May 18, 2021, accepted May 27, 2021, date of publication June 3, 2021, date of current version June 22, 2021.

Digital Object Identifier 10.1109/ACCESS.2021.3085705

IoT Technology-Based Protection Scheme for MT-HVDC Transmission Grids With Restoration Algorithm Using Support Vector Machine

ABDELFATTAH A. ELADL[1], MOHAMMED A. SAEED[1], BISHOY E. SEDHOM[1], (Member, IEEE), AND JOSEP M. GUERRERO[2], (Fellow, IEEE)

[1]Electrical Engineering Department, Faculty of Engineering, Mansoura University, Mansoura 35516, Egypt
[2]Center for Research on Microgrids (CROM), Department of Energy Technology, Aalborg University, 9220 Aalborg, Denmark

Corresponding author: Bishoy E. Sedhom (eng_bishoy90@mans.edu.eg)

ABSTRACT This paper proposes a protection scheme for multi-terminal high voltage direct current (MT-HVDC) transmission grids. The proposed scheme is based on three protection levels; *di/dt* overcurrent protection as the main protection, *dv/dt* undervoltage protection as a backup one protection. If the main and backup one fails to detect and clear the fault current, then the fault tripping and clearing is accomplished using the overcurrent protection by AC circuit breakers (ACCBs) in the AC grid side after a coordinated time. The tripping in the main and backup one protection levels are based on using fault isolation devices (FIDs) tripping. Support vector machine (SVM) is proposed for the fault detection and discrimination in the MT-HVDC using the backup two protection system. The Internet of things (IoT) has been used for monitoring and coordination between the AC grid and MT-HVDC grid. The proposed protection scheme is applied and verified on the MT-HVDC network under different transmission system faults using the MATLAB/Simulink® environment. The results show that the proposed scheme's effectiveness as a fast and reliable scheme in fault detection and discrimination for the MT-HVDC grids.

INDEX TERMS MT-HVDC, di/dt protection, dv/dt protection, MT-HVDC restoration, the IoT, SVM.

I. INTRODUCTION

The operation speed of the protection system for the MT-HVDC transmission grids is considered the main challenge. The converter station's control system is compromised or destroyed by the rapid rise in fault current and may not block such huge fault currents. Furthermore, due to HVDC transmission lines' low impedances, identifying the faulted segment and faults position routines face severe difficulties in such systems [1]. So, it is essential to rapidly detect, identify, and isolate only the faulty section. Therefore, a quick protection algorithm is necessary for primary protection, usually taking less than 1–2 ms concerning the delay in operation time [2]. The faults can be categorized in the MT-HVDC as follows:

- *AC side faults*: Any fault occurs in the AC side (generator, lines, loads, etc.) protected by grid-connected converters, which form part of the AC system's protection design.
- *Internal equipment faults*: The equipment internal faults include failure of electronic devices, filters, etc. Many research efforts have been made to protect the system from potential faults in terms of fault tolerant voltage source converters (VSCs) by providing a backup converter or redundant devices.
- *HVDC network faults*: The most significant MT-HVDC faults are the transmission network fault with parallel related VSCs. Due to the large VSC filter capacitor and cable's low impedance, the transmission network fault causes overcurrent and undervoltage. VSCs' freewheel diodes are subject to overcurrent and can't provide protection against DC side faults. To develop an efficient and secure scheme, these factors need to be analyzed in depth.

In recent years, different protection schemes for the MT-HVDC transmission system have been suggested by many researchers. The most common protection techniques of MT-HVDC grids rely on current or voltage measurement for overcurrent protection, undervoltage protection, differential protection, artificial intelligence-based protection,

The associate editor coordinating the review of this manuscript and approving it for publication was Shaohua Wan.

or distance protection using the traveling-wave (TW) theory propagation [3]. The current and voltage derivatives are local measurement-based protection schemes. It allows the circuit breakers to instantaneously issue a trip signal without delay time because of the locally measured voltage and current values. It is a reliable and fast method in detecting the fault in the MT-HVDC system without any system load interrupting. The current and voltage derivatives are also proposed to distinguish between the internal and external faults based on the sign of the derivatives [4].

A. RELATED WORK

In steady-state cases, the differential algorithm offers high accuracy for fault detection and perfect selectivity [5]. A communication channel between both ends of the transmission line is needed, where there are still problems with communication reliability. An incorrect decision can also be made due to distributed capacitance currents, which can adversely affect the relay's performance [6]. The algorithm presented in [7] used TW and differential protection fault localization approaches based on optical sensors for long and extra-long distance lines. For fault detection, the discrete wavelet transform (DWT) technique has been used. The differential protection performance is enhanced in [8] by using low-pass filters at the line terminals after compensating the distributed capacitive current. However, this technique takes more than 5 ms to isolate the solid faults and a more significant period for faults with high resistance. Besides, to build suitable low-pass filters, an accurate determination of the line section's parameters is required.

A current derivative protection technique based on propagation properties of the initial line-mode voltage TWs is employed in [9] to detect HVDC line faults. The DC line inductors limit the current rate of change; however, DC inductance boosts the DC circuit breaker (DCCB) energy requirements. Authors in[10] proposed a robust protection framework based-on fault-blocking converter. A transient voltage in time-domain with varying sampling times is built to conform to high fault resistances' attenuation and the characteristic of grid band-stop. An enhanced transient TW depend on direction criterion is suggested in [11] to increase the proposed protection scheme's acting sensitivity and efficiency.

The protection technique based on voltage magnitude is presented in [11], which uses its derivatives to classify and isolate HVDC transmission grids' faults. But, the precision of this technique deteriorates with reducing sampling frequency. In [12], mechanical DCCB-based protection is suggested for primary protection with fault clearing times of 60 ms, while after a delay of 20 ms, backup protection is operated. This presented relaying algorithms for HVDC grids do not adequate with selectivity for high operating speeds. The work proposed in [13] placed a current limiting inductor at the two ends of each HVDC line used to realize faults. Simultaneously, these criteria are extremely sensitive to the rate of signal sampling and noise of measurements. It should also be noted that a large inductor would have a considerable impact on the behavior of faults and can result in an unwanted oscillation of DC voltages [14]. Moreover, for internal and external fault discrimination [15], high-frequency TW energy, parameter identification, and magnitude of fault current are also used.

For high-speed single-end protection of MT-HVDC lines, a series inductor is utilized in [16] to filtered the TWs produced by the fault at the faulty line ends. The filtered waveform of voltage processed by a morphological gradient, followed by a decrease in fault voltage, is employed. With an applicable sampling rate, a protection technique based on communication-less for MT-HVDC transmission grids is proposed in [17]. Via tracking the measured change rate of the ratio between current and voltage at all lines and nodes, the suggested scheme detects and identifies the fault. The authors in [18] and [19] proposed a single-ended fault detection technique based on the rate of attenuation of the initial voltage TW in the frequency-domain. The TW quantities produced by external and internal faults are determined, respectively, based on the four-terminal MT-HVDC grid equivalent model. Then, depending on the low-frequency ratio to its high-frequency component amplitude of the original voltage TW, a criterion for distinguishing external and internal faults is built.

The voltage or current derivative may be utilized to increase the speed of network protection [20]. However, it may be affected by the transient faults associated with it. At a time, less than 1 ms, a rapid detection protection scheme for HVDC line faults was suggested in [21]. Authors in [22] presented a reliable protection scheme for HVDC grid faults based on the DC reactor voltage rate of change to improve the detecting accuracy, fault identification and isolating, system robustness, and protection reliability with a fast speed. Even though the HVDC line faults were detected during 1.4 ms, the busbar faults were not detected. Three independent fault criteria were presented in [23] based on wavelet analysis and voltage amplitude. This makes the protection scheme more effective and quicker, where the fault is isolated within 1 ms; however, this technique only detects DC line faults.

The HVDC line's pilot protection using a polarity comparison of the initial current TW is proposed in [24]. The current differential theory for DC line and busbar protection is used. The busbar fault can be observed within 2 ms, while the DC line fault can be detected within 3 ms by that algorithm. Many issues affect TWs, including noise, border distortion, ground faults of high resistance, close-up faults, lightning-induced transients, and multiple DC line terminations. With the assistance of rapid processing tools for digital signals, wavelet analysis can analyze and synthesize information useful in transient signal studies [25]. In HVDC network, the voltage drop is only due to the effect of cable resistance, since the voltage drop due to cable reactance is less dominant; thus, the propagation of faults in the HVDC network is also quick. One of the causes of the protection system's failure during faults is the high current growth rate.

In [26], an algorithm is suggested to detected the HVDC line fault within 6.5 ms using border waves. Regrettably, the busbar faults cannot be detected. Besides, it suffered from numerous technological shortcomings in terms of sensitivity, and a high rate of sampling is required. High-frequency transients were used in [27] for MT-HVDC grids with high-speed fault detection during 0.1 ms to detect DC faults only. Based on the DWT, this technique captures the high-frequency components relevant during the fault. However, it required a very high rate of sampling. It is also significantly impacted by the location of the fault, time of initiation of the fault, fault resistance, and parameters of the HVDC system. The frequency-spectrum correlation is utilized in [28] to detect faults in the HVDC transmission network. This protection technique is based on the estimation of the degree of similarity of the frequency-spectrum between the current of a line and the voltage of another. Based-on the energy ratio between the forward and the backward TWs, a protection scheme based-on permissive pilot suggested in [29]. Just a logical signal from the remote end is required for the proposed security scheme, therefore, eliminating the heavy workload of data sharing and synchronization. On the other hand, communication-based methods can provide selective and fast protection strategies without using any complex algorithm [30]. However, the communication channel represents a main element in the communication assisted methods [31], [32], where it effects on the overall system reliability and cost.

In recent years, the Internet of Things (IoT) has covered various applications as rendering smart elements of daily life and creating new ones so that smart communities, smart agriculture, and smart business ventures can be realized. IoT technologies such as phasor measurement units (PMUs), smart metering, and two-way communication are essential tools for tracking and managing all power grid variables in real-time to perform flexible and intelligent power system operation. IoT enables the power system to exchange information between the participants, increase efficiency, and strengthen the communication of the power system components.

Many applications in smart power grids based on IoT technologies, which including, but not limited to real-time monitoring and control system [33], medium-voltage protection of smart grid [34], protection of distribution networks [35], and protection and control of microgrids [36]. The power grid's operation and protection require faster sensing, communication, and switching systems. The communication system represents an expanded development of the previous implementation mentioned in [37]. But, the use of IoT opens the door for cyberattacks; Cybersecurity has become one of the most relevant IoT fields with the increasing possibility of cyberattacks. IoT security aims to reduce cybersecurity risk to organizations and users by protecting IoT assets and privacy by various technologies and protocols [38], which cannot be overlooked by all those interested in this field.

Support vector machine (SVM) based approach as a dual-functional classifier is introduced in [39] to detect and classify grid fault and islanding events in the power grid. Authors in [40] suggested a hybrid fault diagnostic strategy that uses SVM and enhanced particle swarm optimization (PSO) to perform additional diagnostics based on qualitative reasoning. A technique for fault source detection and identification of wind farm high-voltage trip-offs is proposed in [41] based on multi-dimensional attribute indices and the PSO-SVM method. The PSO method is utilized in the hyper-parameters SVM optimization for better classification performance in the unbalance and balance mode, single and/or compound fault source identification. Authors in [42] proposed a fault detection technique based on SVM in the multi-modular converter HVDC system for the quick recovery of the faulty line, particularly for high-resistance grounding faults. Recently, a hybrid PSO-SVM technique with good efficiency and higher accuracy [43] is used for the distribution system series arc fault detection under different load type conditions. A fault diagnostic system for bearing wind turbine gearbox based on PSO-SVM is proposed in [44].

A protection scheme base on SVM to determine the faulty point in modular multilevel converter HVDC transmission line is proposed on [45]. Ref. [46] proposed the SVM-based protection algorithm so that DC faults could be identified, classified, and located in MT-HVDC systems. A protection scheme based-on SVM is proposed in [47] for hybrid AC-HVDC transmission line integrated with a wind farm. A Discrete Fourier Transform is utilized for estimation of the fundamental component of current and voltage signals which are then fed as input to the SVM based fault detector and classifier. A total of three SVM classifier modules have been developed, for performing the tasks of fault detection, identification of fault phases and faulty section.

Table 1. show a comparison of the proposed strategy with existing methods in the related literature.

B. CONTRIBUTIONS AND PAPER ORGANIZATION

This paper proposes an IoT technology-based protection scheme for MT-HVDC transmission system grids with restoration algorithm using SVM. The proposed protection scheme is based on three protection levels; *di*/*dt* as the main protection, *dv*/*dt* as a backup one protection. Besides, the overcurrent relays in the AC side are considered as a backup two protection. The primary protection can clear the fault after a definite time to avoid transient faults. If the main protection fails to clear the system fault, the backup one protection is operated and clear the fault. However, the fault cleared using backup two when the primary and backup one protection fails to clear the fault. The backup two disconnect the MT-HVDC grid, and then the SVM is proposed to discriminate the faulty line and open the fault isolation devices (FIDs) of the faulty line only. The healthy lines' restoration process depends on the PSO method to maximize the restored load and minimize the power loss. The coordination between the three protection levels is based on coordinated time and MT-HVDC fault current level.

TABLE 1. A comparison of the proposed strategy with existing methods in the related literature.

Ref.	Year	Protection Scheme	Algorithm Used	Technology to Communicate	Sampling Frequency	Fault Clearing Time
[6]	2017	Differential currents	Multipoint optical current sensing		2.5 kHz	3–4 ms
[7]	2020	Differential current	DWT	Optical fiber	–	1 ms
[8]	2018	Voltage and current signals at both sides	–	–	4.8 kHz	8-15 ms
[16]	2019	Voltage drop travelling waves	Voltage morphological gradient	–	20 kHz	1 ms
[17]	2019	The rate of change of the current–voltage ratio	Summation and direction of the currents of all branches	–	20 kHz	0.25 ms
[18]	2021	The rate of attenuation of the initial voltage TW	Wavelet Transform	–	25 kHz	3 ms
[22]	2017	The change rate of DC reactor voltage	–	–		1–4 ms
[23]	2011	Voltage amplitude.	Wavelet Analysis	–	20 kHz	1 ms
[24]	2018	Initial current travelling wave Current differential	DWT	–	10 kHz	3 ms
[25]	2020	Current detection	Wavelet Transform	–	50 kHz	-
[27]	2018	High frequency transients created in the current signals	DWT	–	204.8 kHz	-
[28]	2018	Voltage de-coupling method	Frequency-spectrum correlation	–	20 kHz	3–4 ms
[29]	2020	Energy ratio between the backward traveling wave and the forward traveling wave.	Permissive pilot	–	100 kHz	2-5 ms
[31]	2016	Differential current	DWT	–	100 kHz	4 ms
[42]	2019	Voltage signal	SVM-PSO	–	20 kHZ	-
[45]	2021	Voltage fault traveling wave	SVM	–	20 kHz.	-
[46]	2020	DC Voltage and DC Current Analysis	SVM	–	–	0.15 ms
[47]	2020	Time-domain current and voltage signals	SVM-Discrete Fourier Transform	–	20 kHz	-
Proposed work	2021	Differination current and voltage	SVM-PSO	IoT-LoRaWAN	100 kHz	1.22 ms

The first and second protection levels are based on local measurements from voltage and current transducers in the MT-HVDC grid, and hence, it does not require any communication channels. However, an IoT framework has been proposed in these two levels for current and voltage sensing, FIDs status monitoring, and transmitting data to the master control center. In the third protection level, the IoT technology has been used for data monitoring from the voltage and current transducers in the MT-HVDC side and the AC grid side, transmitting data to the master control center, sending a control command to open the faulty line identified by the SVM algorithm, and restoring the healthy lines depending on PSO method to ensure the system stability. The communication-based IoT relies on the Long-Range Wide Area Network (LoRaWAN) technology. In contrast, the IoT technology is based on a data distribution service (DDS) protocol for message transferring between the connected FIDs, AC circuit breakers (ACCBs), voltage and current transducers in both MT-HVDC and AC sides, and master control center. The proposed scheme has been tested on a hypothetical MT-HVDC grid under different fault conditions, including; pole-to-ground (P-N), pole-to-pole (P-P), and pole-to-pole to ground (P-P-N).

The main contribution of this paper can be summarized as follow;

- Proposing a protection scheme based on di/dt as the main protection, dv/dt as a backup one protection, and AC side overcurrent relays as a backup two.
- SVM based classification method is proposed to identify the faulty line in the MT-HVDC grid.
- Proposing restoration process for the healthy lines based on the PSO technique to obtain an optimal restoration sequence to maximize the restored load and minimize the power loss.
- Applying the IoT technology to communicate between the ACCBs in the AC side and the FIDs in the MT-HVDC grid using LoRaWAN communication channel and DDS messaging protocol.

The rest of the paper is organized as follows; Section II presents the proposed IoT framework. Section III discusses the proposed protection strategy for MT-HVDC transmission grids, and Section IV explains MT-HVDC transmission grids restoration using the SVM algorithm. Section V discusses the MT-HVDC modeling, and Section VI presents the simulation results and discussion. Finally, the paper is concluded in section VII.

II. PROPOSED IoT FRAMEWORK

IoT Messaging Protocols are used to transfer telemetry (or messages) from IoT devices to IoT messaging hubs

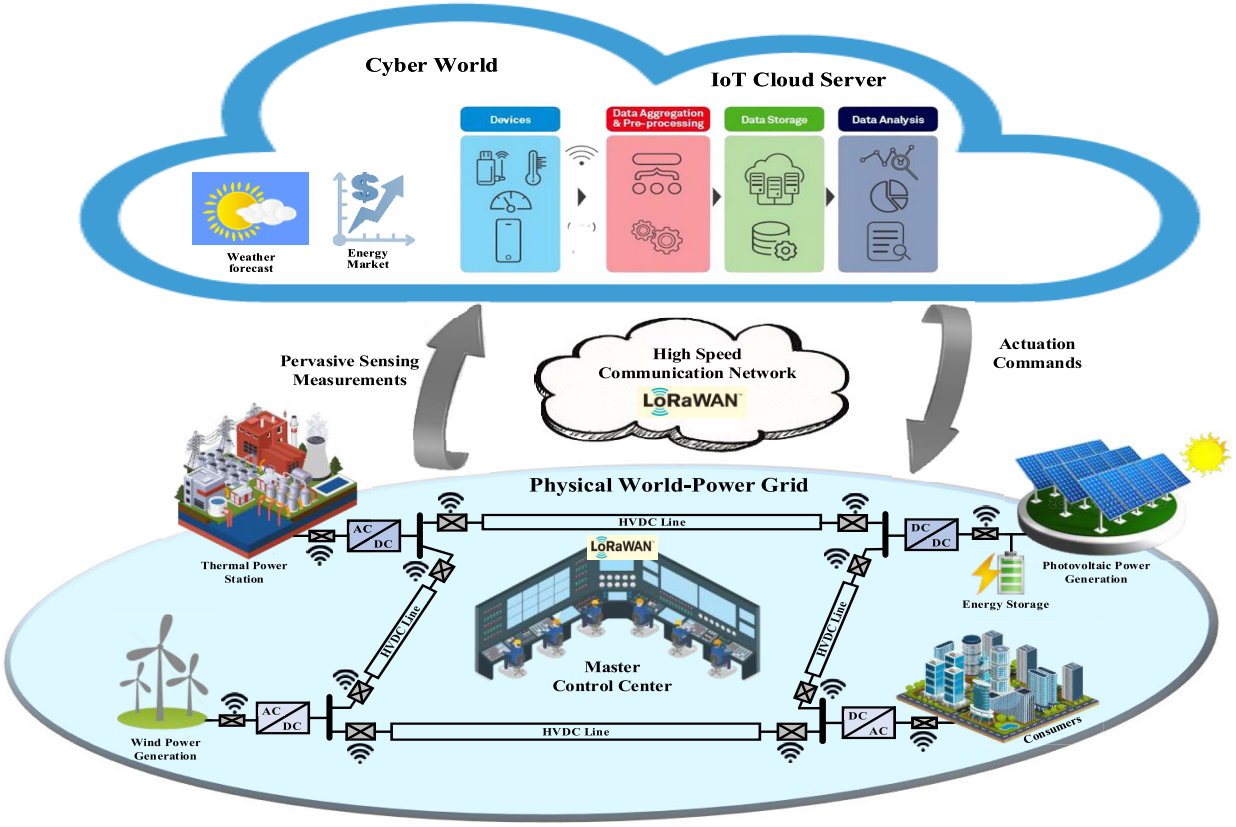

FIGURE 1. The proposed IoT framework.

(or broker). Connecting IoT devices to a network, the Internet, or even each other may use one of a variety of methods. IoT devices may be connected via WiFi, Bluetooth, ZigBee, and Cellular, or other communication methods. Once the IoT solution elements are connected, a message protocol will transmit device telemetry to and from the connected devices. Fig. 1 represents the proposed IoT framework.

A. IoT COMMUNICATION ARCHITECTURE

A variety of communication infrastructures for real-time IoT applications have recently been introduced in several fields, each with its own specific needs. The choice of communication technology for a specific sensor depends on the technical characteristics, the real site environment's condition, the availability of the communication networks, and the power supply. In this work, the LoRaWAN technology is utilized to coordinate dispersed interface protection systems. LoRaWAN designed to provide long-range communication, low-cost, easy deployment, appropriate coverage capabilities, enhanced energy-efficient, indoor penetration and end-to-end, and bidirectional connectivity for IoT applications. It is based on Long-Range applications such as smart cities, smart homes, and smart grids, etc. [34], [48]. There are several authentication procedures [49] such as; one-way authentication, two-ways authentication, and three-ways authentication. In our manuscript, three-way authentication where the control center uses a centralized server or a trusted third party to authenticates the two parties and helps them to mutually authenticate themselves.

B. IoT MESSAGING PROTOCOLS

The widely used communication standard IEC 61850 suggests the use of the Manufacturing Message Specification (MMS) communication protocol for the Local Area Network and DDS protocols for the Wide Area Network (WAN).

In this paper, the DDS protocol for data-based collaboration middleware is used. The DDS is chosen by the smart grid interoperability panel to enable the smart grid to perform the interoperability, which is defined as the capability of two or more systems, networks, devices, applications, or components to easily communicate, share, and use information securely and efficiently with little or no inconvenience to the user [50]. DDS interlinks all system components and provides real-time communication. Besides, it ensures low-latency data access, high-performance, extreme reliability, dependability, scalability of data exchange, and a modular architecture required for the enterprise and mission-critical IoT applications DDS provides a standard application programming interface for C, C^{++}, Java, and.NET for flexible integration with multiple applications.

Fault protection and detection can be achieved using IEEE 802.11n WLAN or Ethernet in conjunction with IEC 61850. The decentralized approach is intended to share and

exchange information between the FIDs, ACCBs, current and voltage transducers, and the master control unit [51].

III. PROPOSED PROTECTION STRATEGY FOR MT-HVDC TRANSMISSION GRIDS

In this paper, a three levels protection strategy is proposed: *di/dt* overcurrent as the main protection, *dv/dt* undervoltage as a backup one, and the backup two is the tripping from the overcurrent protection on the AC grid side using ACCBs. The coordination between the three protection levels is based on time (Δt) and the level of fault current (ΔI). It is proposed that the FID is used in the MT-HVDC transmission grids to eliminate the faulty lines based on solid-state technology. The communication network between the different FIDs in the MT-HVDC grid and the ACCBs depends on the IoT technology.

The main protection is operated after a definite time delay and at a preset value of the fault current (FC) to overcome the transient conditions in the MT-HVDC transmission grid. The FC rate of change is dedicated from each line after sampling and using an anti-aliasing filter to eliminate the noise and undesirable signals. The derivative current can be calculated using first and second-order derivative techniques as following [4], [52];

$$\frac{di}{dt} = \lim_{\Delta t \to 0} \frac{i\,(t_0 + \Delta t) - i\,(t_0)}{\Delta t} = \frac{\Delta i}{\Delta t}, \quad \Delta i = i_k - i_{k-1} \tag{1}$$

$$\frac{d^2 i}{dt^2} = \frac{d}{dt}\left(\frac{di}{dt}\right) = \frac{d}{dt}\left(\frac{\Delta i}{\Delta t}\right) = \frac{\Delta^2 i}{(\Delta t)^2}, \quad \Delta^2 i = \Delta i_k - \Delta i_{k-1} = i_k - 2i_{k-1} + i_{k-2} \tag{2}$$

where, k is the sampling instant, and i_k, i_{k-1}, and i_{k-2} are the FC present and previous samples at k, $k-1$, and $k-2$ instants, respectively. In the normal and steady-state conditions, the current derivative is equal to zero. However, under the fault conditions, the value of the current derivative is changed. The tripping signal has been sent to the FIDs when the value of the $\Delta^2 i$ exceeds the threshold value. For an accurate representation of the *di/dt* overcurrent protection in the MT-HVDC grid, the sampling time must be approximately $1/10^{th}$ of the minimum time to reach the peak of the FC signal [4].

If the main protection failed to detect and clear the fault, the backup one voltage derivative *dv/dt* protection is used to trip the fault after a coordinated time and at a predefined FC value (ΔI). The voltage signal has been measured at each bus, then these signals have been sampled using a proper sampling frequency. The voltage derivative can be evaluated using the following equation [53];

$$\frac{dv}{dt} = v_k - v_{k-1} \tag{3}$$

where, v_k and v_{k-1} are the present and the previous samples of the voltage signal at instants k and $k-1$, respectively. At steady-state condition, the voltage derivative is equal to zero approximately. However, under fault condition, the *dv/dt* increased over the prescribed threshold value, and hence the relay issue a trip signal to the FIDs in the MT-HVDC grid to disconnect the faulty line.

The selection of the current derivative as a main protection because it has the fast fault detecting speed [54]. It can predict the overcurrent issues earlier than the overcurrent protection, and not constrained by the communication delay compared to the unit protection. Voltage derivative may be used as a main protection and current derivative may be used as a backup. But voltage derivative technique has some challenges regarding sensitivity due to fault loop impedance, directionality, and time delay for healthy conditions [55], [56].

If the main and backup one fails to detect and clear the FC, then the fault tripping and clearing are accomplished using the overcurrent relays in the AC side by ACCBs after a coordinated time. In this protection level, the overcurrent protection in the AC grid side issues a trip signal to the ACCBs to disconnect the MT-HVDC grid with all its lines. A discrimination process is then performed to eliminate only the faulty line and restore all other healthy lines' steady-state operation. This discrimination process is based on the SVM classification method, presented in detail in the next section.

The flowchart that illustrates the fault clearing process using the proposed protection scheme is shown in Fig. 2. Fig. 3 presents the coordinated time between the main, backup one, and the protection scheme's backup two protection levels. The required time for fault clearing, t_{fc}, is composed of three-time intervals. The first is the time required for the fault detection and identification, t_{fd}. The second is the time for the FIDs to interrupt the fault, t_{fb}, and the third time is the fault current interruption, t_{fi}. The following equation represents the fault clearing time.

$$t_{fc} = t_{fd} + t_{fb} + t_{fi} \tag{4}$$

IV. MT-HVDC TRANSMISSION GRIDS RESTORATION USING SVM CLASSIFICATION ALGORITHM

The discrimination process starts after a coordinated time when ACCBs operate and isolate the MT-HVDC grid. A discrimination process that depends on SVM is proposed to detect the faulty line from the MT-HVDC grid and then reconnect the health lines. The method of detecting the faulty line is considered a pattern classification problem. SVM depends on statistical machine learning theory. It is applied to minimize the structural risk, enhance generalization ability, and balance the experience, risk, and confidence range considering limited data sampling [40]. The SVM's basic concept is to obtain an optimal hyperplane that separates between two data classes with the maximum separation margin in a high dimensional space [57]. Firstly, the data are measured at all buses in the MT-HVDC grid; then, the data are clustered to identify the faulty line. After determining the faulty line, the two FIDs in the faulty line are tripped and then isolate the faulty line out of the service. The rest of the healthy transmission lines are

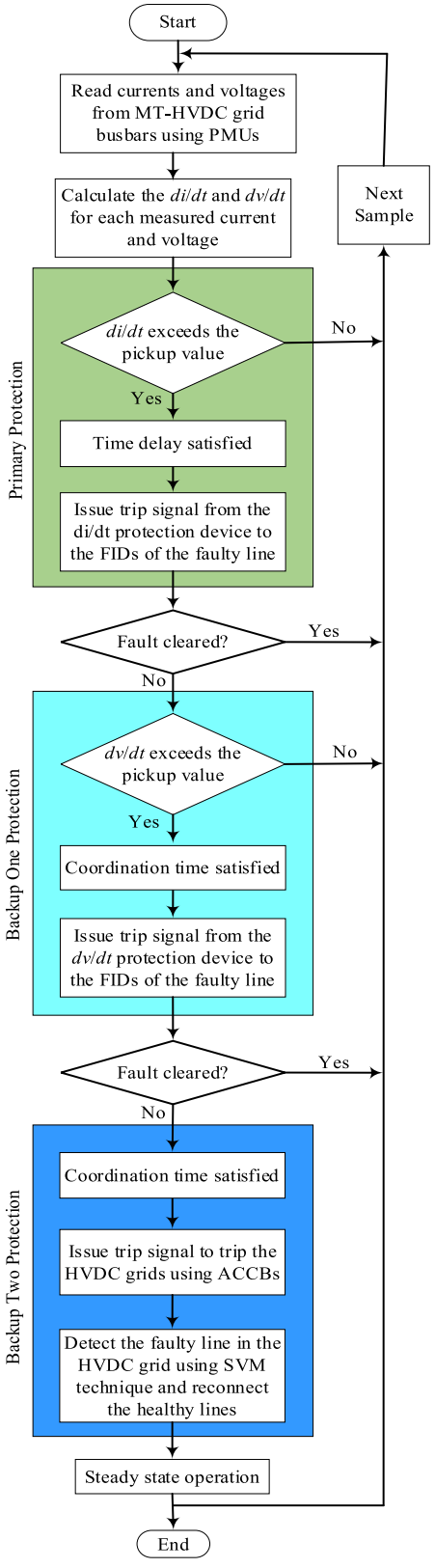

FIGURE 2. Flowchart of the proposed protection scheme.

reconnected to the service to supply the system load demand. The measured current and voltage data are transferred via a communication channel to the master control center.

In the restoration process, the IoT based communication channel has been proposed to interlink between the overcurrent relays in the AC side, voltage and current transducers, ACCBs, FIDs, and the master control center. The proposed communication channel is depending on LoRaWAN communication network and DDS messaging protocol. The IoT technology has been used for data monitoring from the voltage and current transducers in the MT-HVDC side and the AC grid side, transmitting data to master control center, sending a control command to open the faulty line identified by the SVM algorithm, and restoring the healthy lines depending on PSO method to ensure the system stability. The speed and reliability of this restoration algorithm are affected by the accuracy of the communication channel.

The SVM decision is to identify and detect the faulty line in the MT-HVDC grid and restore the healthy lines to ensure the system's steady-state operation. The SVM block used for data training contains three values; hence, the kernel level is three, and the SVM classification is in four-dimensional space. The hyperplane in the $\Re^n$ with n-dimensional space is $n-1$ dimensional subspace [39]. Accordingly, the selection of the margin is another priority task to ensure a successful data classification process. It is necessary to choosing large margins to tackle the miss-classification of the input data. For obtaining a convenient kernel, all input signal data must be measured, namely, current and voltage at each bus in the MT-HVDC grid. In this classification problem, the kernel level is four, and it is necessary to do a kernel trick that is a sub-process of choosing a proper hyperplane. The SVM is performed to select a convenient hyperplane that follows the structural risk minimization principle. Given a set of the trained data $s=\{(x_i, y_i)|\, x_i \in \Re^n, y_i \in \Re\}_{i=1}^{n}$, the SVM based on kernel classification decision function can be written as follows [58];

$$f\,(x) = sign\left\{\sum_{i=1}^{N} \alpha_i y_i k\,(x_i, x) + \beta\right\} \tag{5}$$

where $sign\{\ \}$ is the sign function, x_i is the i^{th} image of the support vector, y_i is the classification label where $y_i \in \{-1, 1\}$, and N is the number of the sample. α_i and β are the SVM weighted parameters in the feature space and the bias, respectively. Where, $k\,(x_i, x)$ is the kernel function that can be represented as a Gaussian function follows [58];

$$k\,(x_i, x) = e^{\left\{-\frac{|x-x_i|^2}{\sigma^2}\right\}} \tag{6}$$

where $\sigma \in \Re$ that represents the Gaussian width. Hence, the SVM classification function can be described as follows;

$$f\,(x) = sign\left\{\sum_{i=1}^{N} \alpha_i y_i exp\{-|x-x_i|^2/\sigma^2\} + \beta\right\} \tag{7}$$

Gaussian kernel is used with appropriate regularization guarantees a globally optimal predictor which minimizes both the estimation and approximation errors of a classifier. It is more flexible and supports infinitely complex models.

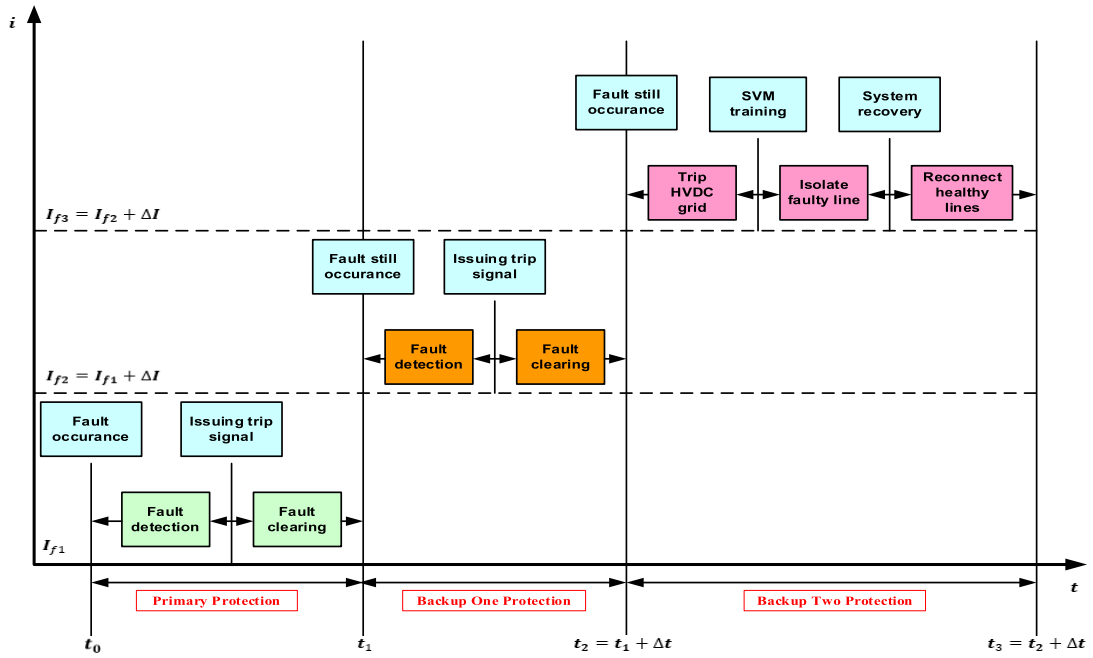

FIGURE 3. Coordination time for the three protection levels.

The absolute value of the function $f(x)$ represents the distance between the corresponding sample and the separating hyperplane. If the function $f(x)$ is positive, and its absolute value is large; hence the system is stable. However, if the function is negative with a large absolute value, the system is considered unstable, and therefore the faulty line is detected and disconnected from the service. Accordingly, the function $f(x)$ can be considered as a fault detection index. Fig. 4 represents the basics of the SVM classification method.

The system load restoration has been performed under two constraints: the line capacity and the operational constraints. The main objective is to minimize the load shedding and total power loss while preserving the load and generation's operational constraints and power balance. The main objective function can be written as follows;

$$min \left\{ P_{shedding}, \sum_{m,k \in B} P_{mk,t} \right\} \tag{8}$$

Subject to the following constraints;

$$\sum_{i \in G} P_{gi,t} - \sum_{j \in D} P_{dj,t} = \sum_{m,k \in B} P_{mk,t} \tag{9}$$

$$\left(P_{mk,t}\right)^2 + \left(Q_{mk,t}\right)^2 \leq \left(S_{max\ mk,t}\right)^2 \tag{10}$$

$$|I_{l\ min}| \leq \left|I_{l,t}\right| \leq |I_{l\ max}| \quad l \in L \tag{11}$$

$$|V_{n\ min}| \leq \left|V_{n,t}\right| \leq |V_{n\ max}| \quad n \in B \tag{12}$$

$$P_{gi\ min} \leq P_{gi,t} \leq P_{gi\ max} \tag{13}$$

where, G, D, and B are the set of generators, loads, and buses in the system respectively, $P_{gi,t}$ is the active power generation of the i^{th} generators at time instant t, $P_{dj,t}$ is the active load

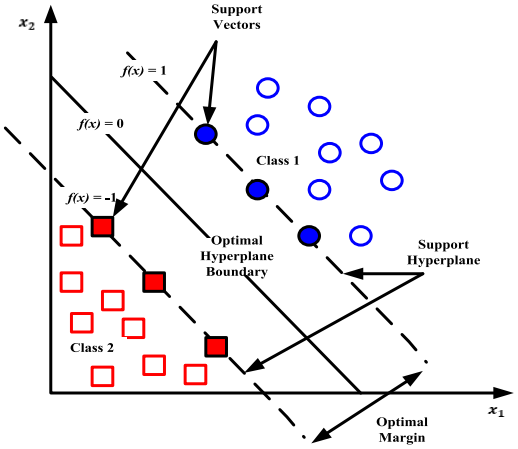

FIGURE 4. SVM basic principle for classification problem.

power at time t, and $P_{mk,t}$ is the active power flow in the line between bus n and k. According to the active, $P_{mk,t}$, and reactive, $Q_{mk,t}$, power flow in the lines the thermal limit of the system lines, $S_{max\ mk,t}$, is considered in (10). $I_{l\ min}$ and $I_{l\ max}$ are the minimum and maximum of the line current limits and $V_{n\ min}$ and $V_{n\ max}$ are the upper and lower limit of the bus voltage magnitude. While the generators minimum, $P_{gi\ min}$, and maximum, $P_{gi\ min}$, active power outputs are presented in (13).

This problem can be solved using an optimization algorithm based on PSO algorithm. The flowchart of the system restoration process is presented in Fig. 5. The optimal solution is reached concerning the stopping criteria as the maximum number of iteration or the minimum error tolerance.

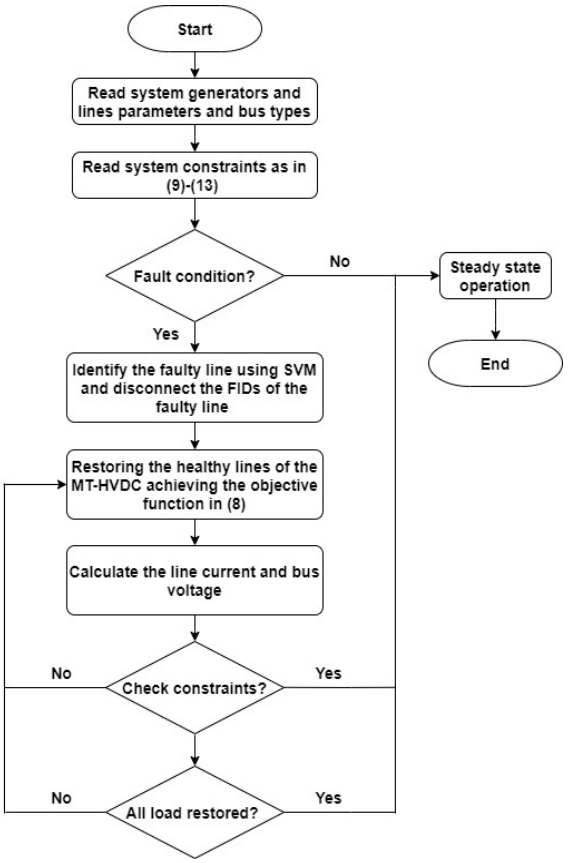

FIGURE 5. Flowchart of the MT-HVDC restoration process.

V. MT-HVDC GRID MODELING

A MT-HVDC grid is built to verify the proposed protection schemes' feasibility and validity where HVDC fault clearance is achieved either using FIDs or ACCBs. The configuration of the proposed MT-HVDC is shown in Fig. 6. The MT-HVDC grid comprises five cables. The chosen lengths of links L1 –2, L1–4, L2–3, L2–4, and L3–4 are 10 km, 50 km, 10 km, 50 km, and 50 km, respectively. Each link end is equipped with FID. The 4-terminal HVDC grid has a symmetrical monopole topology with a ± 135 kV point to point voltage. Three multi-modular converters (MMCs) are used to connect the AC sources with the HVDC grid. However, one MMC is used to connect the HVDC grid with the AC load demand. The controller of the MMC in the generating unit side is composed of two levels; AC-DC rectifier and DC-DC converter. However, the MMC on the load side is composed of a DC-DC converter and DC-AC inverter. The MT-HVDC system parameters, grid cable parameters, and MMC parameters are given in Tables II, III, and IV, respectively.

The schematic diagram that represents the controller used in the MMC is shown in Fig. 7. The MMC controller consists of three control loops, including; the droop controller, the P/Q control loop, and the inner current control loop. The AC voltage and current, v_{abc1} and i_{abc1}, are transformed into dq components, v_{d1}, v_{q1}, i_{d1}, and i_{q1} respectively and

TABLE 2. MT-HVDC network parameters.

Item	Active Power, MW
DC Bus Bar 1 (Microgrid 1)	45
DC Bus Bar 2 (Microgrid 2)	40
DC Bus Bar 3 (Microgrid 3)	40
DC Bus Bar 4 (Load)	110

TABLE 3. Network cable, equivalent π, model parameters.

LINE	R (P.U.)	L (P.U.)	C (P.U.)	RATTING(MVA)
LINE 1-2	0.063	0.0843	0.137	50
LINE 1-4	0.031	0.0714	0.137	45
LINE 2-3	0.070	0.0161	0.0775	50
LINE 2-4	0.035	0.0806	0.0775	55
LINE 3-4	0.025	0.0106	0.0775	65

TABLE 4. MMC converter parameters.

Property	Value
Base Electrical Quantities	
$V_{dc,base}$	135 kV
$V_{ac,base}$	66 kV (L-L)
S_{base}	220 MVA
MMC Specifications	
Rated DC-Link Voltage	± 67.5 kV
Rated AC Voltage	66 kV (L-L)
Submodule Capacitance, C_{sm}	10.48 mF
On (Off) Submodule Resistance	1 mΩ (1 MΩ)
Arm inductance (pu), L_{arm}	0.15 p.u.
Current Limiting Inductor	100 mH
Capacitor Filter	1.05 µF

the active and reactive power, P_1 and Q_1, at bus 1 are also measured. In the droop control loop, the active reference power is obtained based on the DC side voltage v_{dc1} and the reference DC voltage v_{dc1}^{ref}. The reference dq currents, i_{dc}^{ref} and i_{q1}^{ref} are obtained using the P/Q control loop based on proportional/integral (PI) controller. Then the reference dq voltages, v_{d1}^{ref} and v_{q1}^{ref} are obtained using the inner current controller-based PI control. The reference dq voltages are transformed to abc, and the inverter control signal is obtained using pulse width modulation (PWM).

VI. SIMULATION RESULTS AND DISCUSSION

The simulation implementation is performed in this paper using the Real Time Innovation (RTI) connext connectivity framework, custom-built MATLAB classes and DDS Simulink blocks. These blocks are added to the Simulink model, which helps the model to communicate with other DDS members. During the simulation, the MATLAB/Simulink® coder produces C/C^{++} code from the model and the generated code from the DDS blocks conforms to the RTI Connext DDS. This code is then compiled and executed on the platform supported by RTI Connext DDS or RTI Connext Micro DDS framework. The test system has been presented in Fig. 6, and the system parameters are in Tables II, III, and IV.

The model sampling frequency is 100 kHz, where the sampling time is 10 μs [59]. The switching frequency for

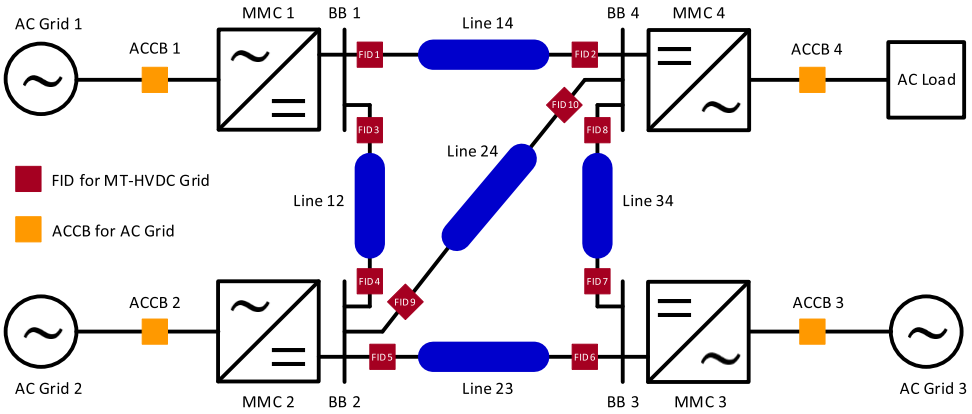

FIGURE 6. Single line diagram of the MT-HVDC transmission grid.

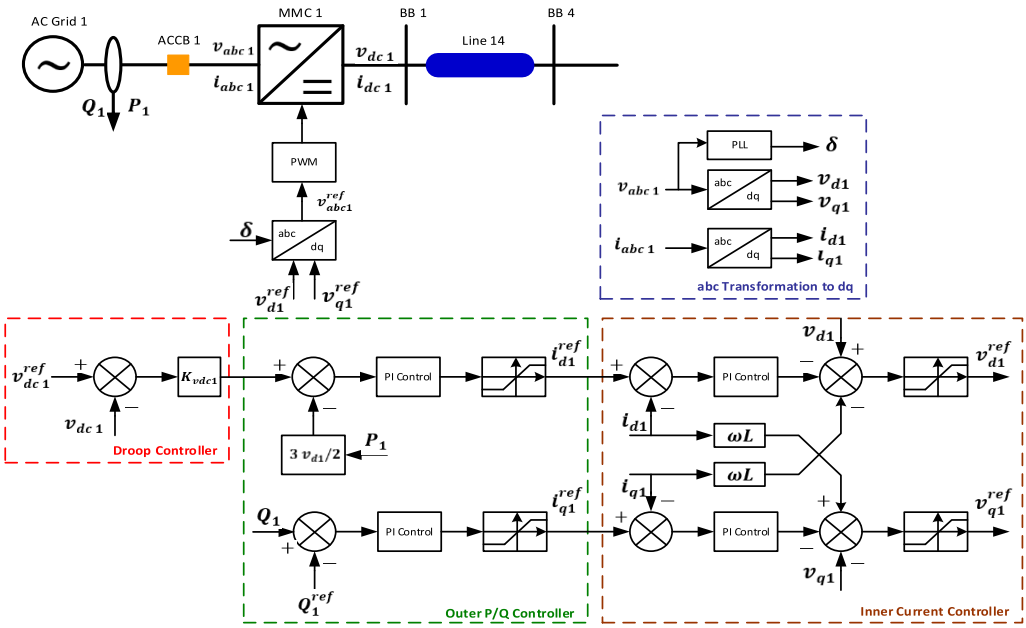

FIGURE 7. MMC controller schematic diagram.

all the connected converters and the FIDs in the MT-HVDC transmission grids can be determined as 10 kHz, which provides a switching time of 0.1 ms [60], [61]. The high sampling frequency ensures the required frequency band needed for the algorithm. The IoT communication platform has been proposed to interlink the ACCBs, the FIDs in the MT-HVDC transmission networks, and the AC side's over-current relays. The communication-based IoT depends on the LoRaWAN communication network The frequency rate of the LoRaWAN technology is 868 MHz [62]. Using this communication channel, the voltage and current measurements, FIDs status monitoring, and the voltage and current derivates values are transmitted using DDS protocol to the master control center.

The proposed scheme has been applied in the presence of the different fault conditions in the MT-HVDC, including pole-to-ground (*P-N*), pole-to-pole (*P-P*), and pole-to-pole-to-ground (*P-P-N*). The system outputs are voltage, current, and active power at each busbar and the voltage and current at the system load. In this section, three scenarios are proposed as follow;

A. Operating the main protection
B. Operating the backup one protection
C. Operating the backup two protection

A. SCENARIO#1 OPERATING THE MAIN PROTECTION

In this scenario, it is assumed that the proposed scheme's main protection can detect the fault in the MT-HVDC grid. When a *P-N* fault has occurred in the line between bus 1 and bus 4 at 3.0 s, the *di/dt* protection scheme trip and clears the fault in the HVDC grid. The fault tripping with the main protection has been done using the FIDs in the HVDC grid. Fig. 8 shows the voltage and current at each bus. At the instant of the fault occurrence, the voltage at each bus is decreased until the FIDs for the line between bus 1 and bus 4 in the HVDC grid are opened, and hence the fault is cleared.

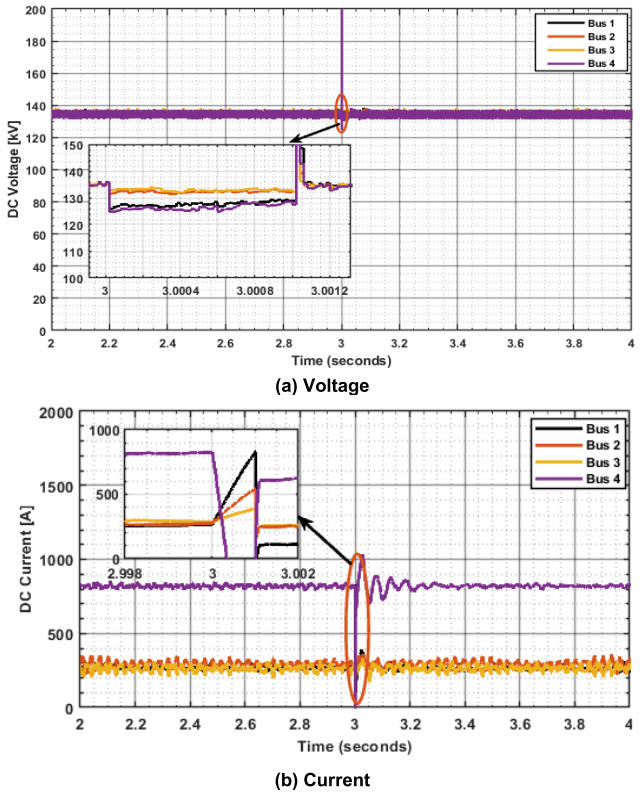

FIGURE 8. (a) Busbars voltage, and (b) busbars current, by applying di/dt protection with P-P fault for scenario#1.

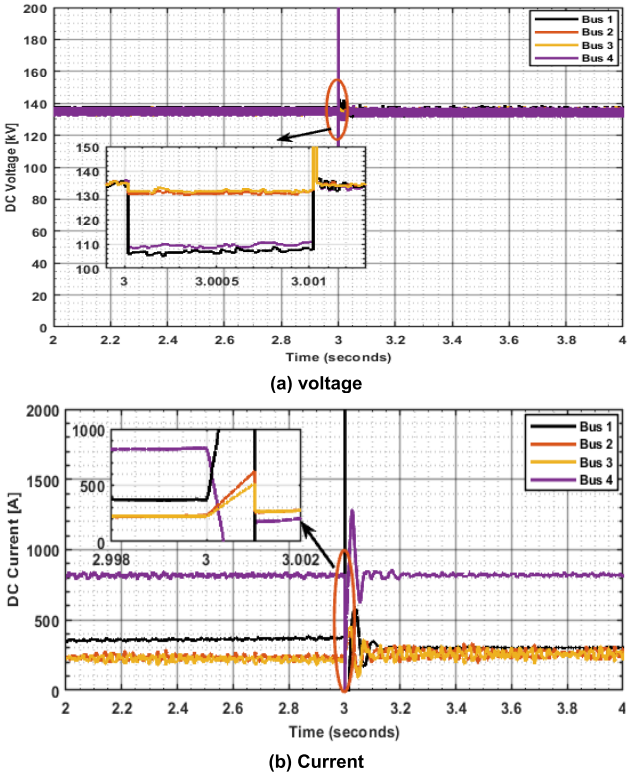

FIGURE 9. (a) Busbars voltage, and (b) busbars current, by applying di/dt protection with P-P fault for scenario#1.

The voltage reduction for bus 1 and bus 4 is more than the other buses where the fault is in the lines between the two buses. The FIDs in the line between bus 1 and 4 are opened after 1.0 ms, and hence the faulty line is tripped from the HVDC grid, and the other lines are stably operated as shown in Fig. 8(a).

However, the current at each bus is increased when the fault occurs. The current increase in bus 1 is more than other buses as the fault occurs in the line between bus 1 and bus 4; meanwhile, the current at the system load bus is increased but in the reverse direction as shown in Fig. 8(b). At steady-state operation, the current of bus 4 is the sum of other buses' currents as it is a load bus. At each MMC, the control system and the protection system's fast operation limit the currents' increase at each bus.

The main protection scheme has been applied to trip a *P-P* fault in line 1-4. The output results at each bus have been presented in Fig. 9 with applying for the *di/dt* overcurrent protection. Fig. 9(a) shows the voltage at each bus, which indicates that the fault occurred at 3.0 s, and the FIDs trip the fault after 1.0 ms. Also, the voltage reduction in bus 1 and 4 is more than the other two buses as the fault is located in the line between these two buses. Fig. 9(b) represents the current at each bus in which the current is increased at each bus; however, in bus 4 it increased in the reverse direction. The *di/dt* protection clears the system fault after 1.0 ms from its occurrence, and then the current flow is changed to supply the system load connected to bus 4.

Also, a P-P-N fault has been applied to the line between buses 1 and 4. The main protection scheme has been verified, and the results have been obtained in Fig. 10. The output results at the buses and load are presented in Fig. 10 with applying the di/dt overcurrent protection. As shown in Fig. 10(a), the primary protection system can clear the fault after 1.0 ms of its occurrence. The voltage on bus 1 and 4 is decreased more than the other two buses. After fault clearing, the voltage at each bus is regulated to its nominal value. Fig. 10(b) shows the current at each bus in the HVDC grid. The current is increased due to the fault in all system buses; however, at bus 4 its direction is reversed. After tripping the fault, each bus's current is shared according to each line's limits in the HVDC grid.

B. SCENARIO#2 OPERATING THE BACKUP ONE PROTECTION

In this scenario, it is assumed that the main protection failed to clear the fault, and the backup one can detect and clear the fault after the coordination time of 1 ms. The backup one protection in the proposed scheme is based on dv/dt protection. Also, the fault is detected and cleared using the FIDs in the MT-HVDC grids. The results are obtained by applying the proposed protection scheme in the presence of different fault conditions.

In the presence of the P-N fault in the line between buses 1 and 4, Fig. 11 shows the output results at each bus and the load results, respectively, by using the proposed protection

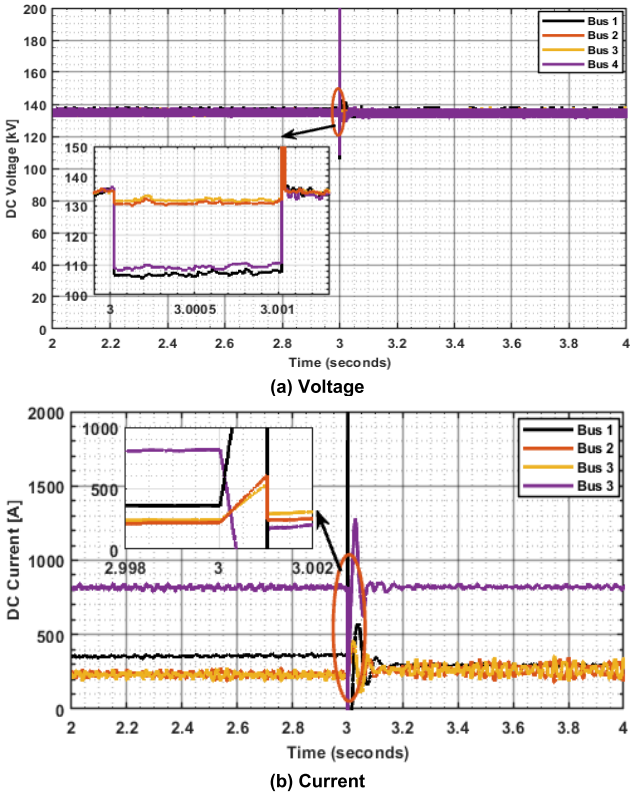

FIGURE 10. (a) Busbars voltage, and (b) busbars current, by applying di/dt protection with P-P-N fault for scenario#1.

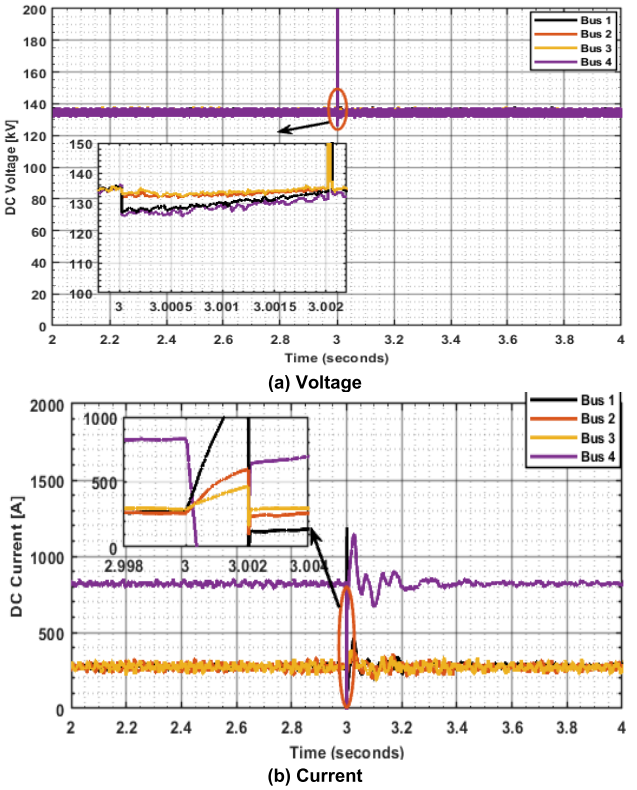

FIGURE 11. (a) Busbars voltage, and (b) busbars current, by applying first protection scheme with P-N fault for scenario#2.

scheme. Applying P-P fault in line 1-4, the obtained bus results and load are presented in Fig. 12 by using the proposed protection scheme. In the presence of P-P-N fault in the same line, the results obtained at each bus and the load are presented in Fig. 13 by using the proposed protection scheme.

In this scenario, the primary protection fails to detect the fault then the backup one dv/dt protection trips the FIDs of the faulty line. The fault also occurred at 3.0 s, and the backup one trip the FIDs after main protection failure at 3.00202 s. In each fault condition, the system voltage decreased as in the first scenario; besides, the current at each bus is increased at the instant of the fault occurring till the FIDs trip. After fault clearance, the current and active power are shared according to the HVDC grid's line limits. The fault occurrence influences the voltage and current of the connected load with small fluctuations until the fault is cleared using the backup one protection in case of main protection failure. The MMC controller adjusts the load voltage and current to their nominal values.

C. SCENARIO#3 OPERATING THE BACKUP TWO PROTECTION

This scenario has been operated if the main and backup one protection failed to detect and clear the fault and after a coordination time 2 ms from the main protection time. This level of the proposed protection scheme is based on the fault detection using the overcurrent protection by the ACCBs in the AC grid. Firstly, the ACCBs have been tripped then; a discrimination method has been applied to detect the faulty line in the MT-HVDC grid, finally connecting the healthy lines to supply the system loads. The results are obtained in the presence of the different fault conditions and by applying the proposed method.

Firstly, the fault is cleared using the overcurrent protection and the ACCB on the AC side; hence, the HVDC grid has been disconnected from the network. Secondly, the SVM has been trained to identify the faulty line to disconnect it from the HVDC grid using the data classification method. The healthy lines are then restored to supply the system load demand by minimizing the load shedding and the power loss while ensuring the power balance, line capacity, and other operational constraints. After disconnecting the HVDC grid, the bus currents are reduced to zero; hence, the restoration process began to reconnect the healthy lines. In this fault, line 3-4 is connected as it is considered the closest line and with small path resistance then, connect lines 2-4, 1-2, and 2-3 respectively. The healthy lines' reconnection's main objectives are to maximize the restored load and minimize the power loss; hence, the closest lines with small resistance are first connected, and then the other lines are restored respectively.

In the presence of the P-N fault in line 1-4, the fault has been tripped using the proposed protection scheme. The voltage and current at buses are presented in Fig. 14. By applying the P-P fault in the same line, the results obtained by using the proposed protection scheme are presented in Fig. 15. While

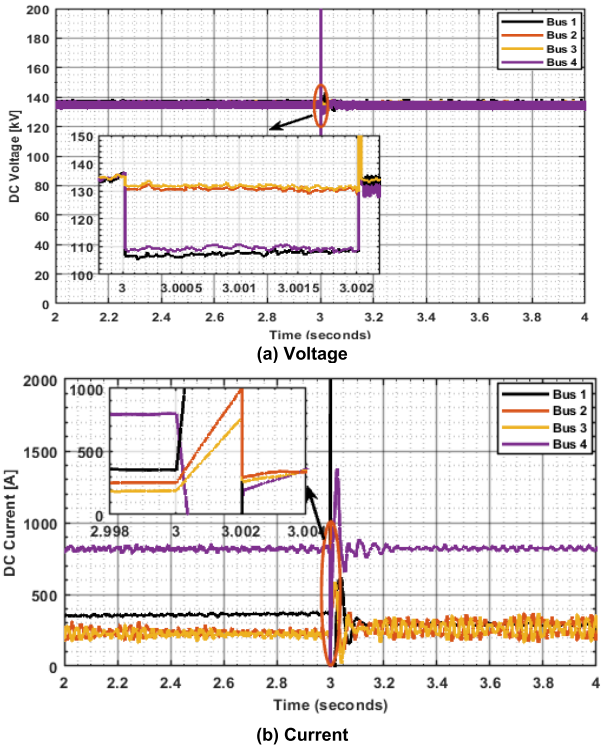

FIGURE 12. (a) Busbars voltage, and (b) busbars current, by applying first protection scheme with P-P fault for scenario#2.

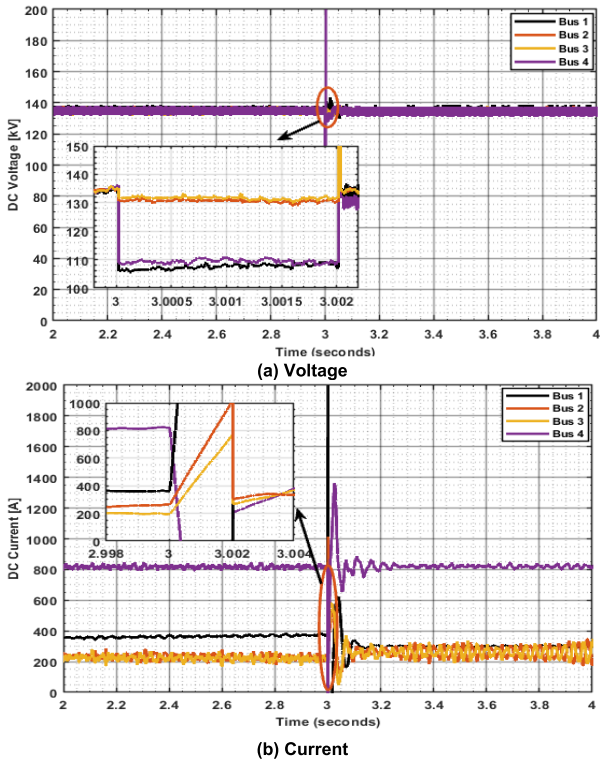

FIGURE 13. (a) Busbars voltage, and (b) busbars current, by applying first protection scheme with P-P-N fault for scenario#2.

in the presence of P-P-N, the results obtained by applying the proposed protection scheme are illustrated in Fig. 16.

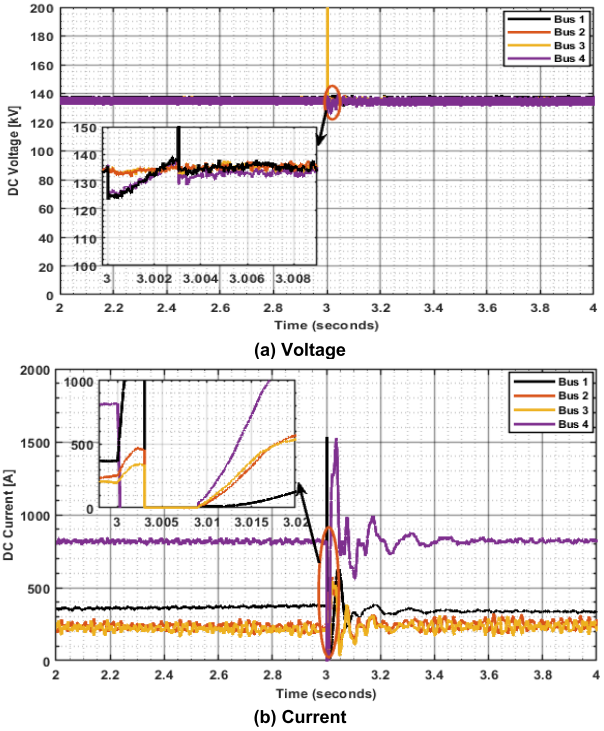

FIGURE 14. (a) Busbars voltage, and (b) busbars current, by applying first protection scheme with P-N fault for scenario#3.

TABLE 5. Clearing time and steady-state operating time with applying the proposed protection.

Item	Clearing Time	Load Steady-State Operating Time
	Applying the Main Protection	
P-N	3.00122	3.20
P-P	3.00122	3.20
P-P-N	3.00122	3.20
	Applying the Backup One Protection	
P-N	3.00222	3.25
P-P	3.00222	3.25
P-P-N	3.00222	3.25
	Applying the Backup Two Protection	
P-N	3.00322	3.40
P-P	3.00322	3.40
P-P-N	3.00322	3.40

In each fault condition, the system voltage decreased as in the first scenario besides, and the currents are reduced to zero at each bus after the disconnection of the HVDC grid. After the restoration of all healthy lines, the active power and current are shared between the grid lines while preserving the line capacity limits. The voltage at each bus and the load voltage and current are reduced after the fault occurrence; however, it doesn't reduce to zero due to the grid's line capacitance.

The clearing time and the load steady-state restoration time have been obtained by applying the proposed protection scheme in the presence of the three fault conditions. Table 5 shows the clearing time and load steady-state restoration time. The clearing time represents the proposed protection scheme response to any fault; however, the steady-state

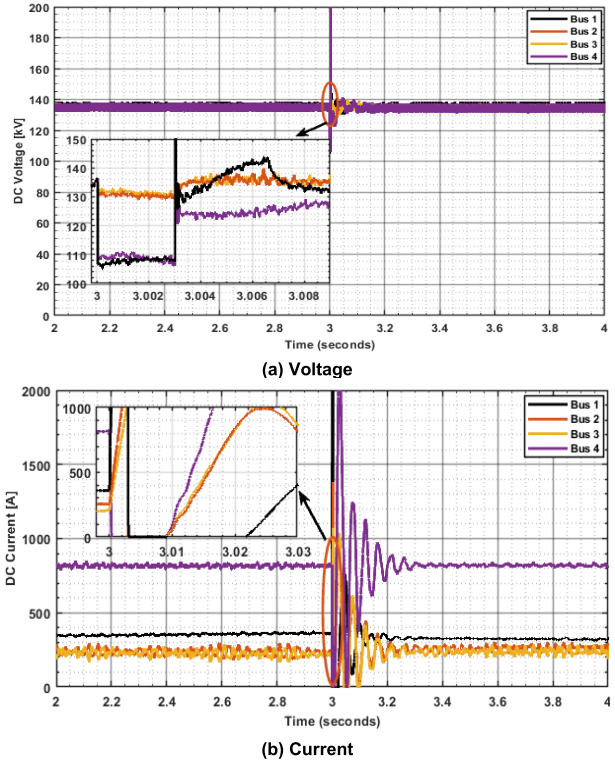

FIGURE 15. (a) Busbars voltage, and (b) busbars current, by applying first protection scheme with P-P fault for scenario#3.

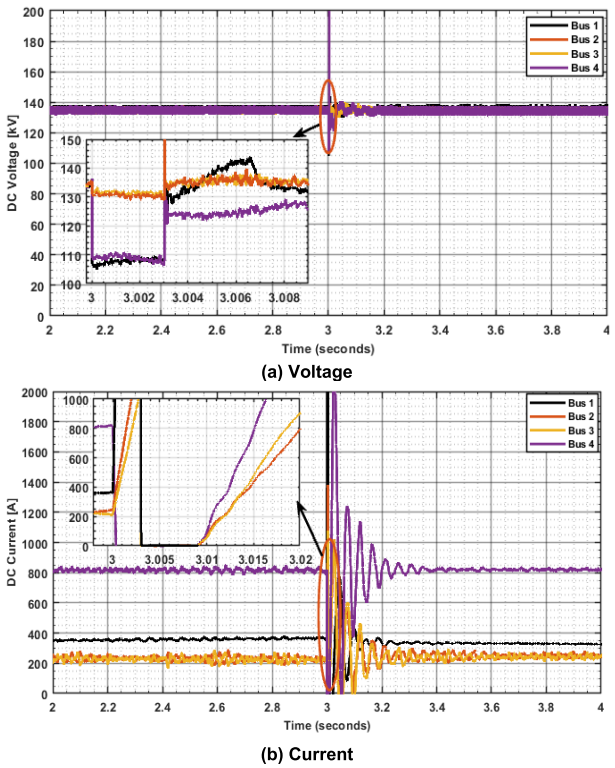

FIGURE 16. (a) Busbars voltage, and (b) busbars current, by applying first protection scheme with P-P-N fault for scenario#3.

operating time represents the time required for the system load to operate in steady-state condition after the fault elimination.

The proposed fault detection method-based SVM involved 8 measured parameters: current and voltage at each bus in the HVDC grid. The main objective is to detect the faulty line in the HVDC grid as fast as possible. The required samples for the discrimination process are samples for the quarter of one cycle post the fault occurrence. The number of samples is 500; hence the entire signal data stack has a 5 ms duration. The samples are stored in a data stack with an operating system based on first-in-first-out. Therefore, the additional new sample is placed on the top of the data stack, and the oldest one is removed from the stack to ensure the data stack up to date for timely faulty line detection. The SVM training algorithm's input is the data stack for all eight parameters for the faulty line detection in the HVDC grid. The whole data for each fault type are 2000 data is divided into 75% of the data for training and 25% of the data for testing and validation. The offline training time is around 75 s of the SVM algorithm for the trained data to detect the faulty line in the HVDC transmission grid. The SVM classification algorithm is trained and tested offline, and the accuracy of the faulty line classification is given as

$$Accuracy = \frac{true\ decision\ for\ faulty\ line\ classification}{tota\ lnumber of\ data}\% \tag{14}$$

TABLE 6. Classification accuracy for the faulty line detection.

FAULT TYPE	TOTAL TEST DATA	TRUE DECISION	FALSE DECISION	ACCURACY (%)
P-N	500	496	4	99.2
P-P	500	497	3	99.4
P-P-N	500	495	5	99.0
Total	1500	1488	12	99.2

Table 6 presents the classification accuracy for different fault types in the MT-HVDC transmission grids. It is to be noted that the true decision from the total test data are 1488 and 12 are the false decision. Hence the accuracy of the faulty line classification process is 99.2 %. The classification accuracy under the different fault conditions P-N, P-P, and P-P-N is 99.2, 99.4, and 99.0%. Also, the SVM classification method provides an overall training accuracy which obtained when trained over training data of about 98.6%.

Table 7 shows a comparison between the proposed SVM, probabilistic neural network (PNN), and adaptive neuro-fuzzy interface system (ANFIS) classifications algorithms. This comparison is based on the training time, faulty line detection time, and classification accuracy. The proposed method has a much lower training and detection time than the other two methods. Also, the accuracy of the proposed method is better than the PNN and ANFIS methods. With small size of the system under study, all optimization techinqyue have the same time, but PSO have many advantages. The offline training of the SVM-PSO takes 75 s however, with the comparison with the ACO, the offline training time is 83 s.

TABLE 7. The comparative results.

METHOD	TRAINING TIME (S)	DETECTION TIME (MS)	ACCURACY (%)
PNN [63]	113	45	95.9
ANFIS [64]	98	40	97.8
The proposed method	75	15	99.2

TABLE 8. The failure simulations on the system's lines and the SVM-PSO solutions.

CASE	OUTAGE LINE				
	LINE 1–2	LINE 1–4	LINE 2–3	LINE 2–4	LINE 3–4
PG1* (MW)	42.475	42.516	42.234	41.987	33.719
PG2* (MW)	28.832	31.421	28.908	27.415	26.320
PG3* (MW)	40.0	40.0	40.0	40.0	40.0
VB4+ (MW)	1.038	1.005	1.041	0.952	0.950
SHEDDING LOAD (MW)	0.0	0.0	0.0	3.21	13.01
POWER LOSS (MW)	1.307	3.937	1.142	2.612	3.039
LINE RESTORATION SEQUENCES	(1-4), (3-4), (2-4), (2-3)	(3-4), (2-4), (1-2), (2-3)	(3-4), (2-4), (1-4), (1-2)	(1-4), (2-4), (1-2), (2-3)	(1-4), (2-4), (1-2), (2-3)

*PG = POWER GENERATION, +VB4 = BUS VOLTAGE.

The outage or failure on the line causes a reduction in the number/percentage of loads supplied in the system, and there are several solutions of closing and opening the switches (CB), which enable to find an optimized restoration of the system. In this work, and when the MT-HVDC grid fully outages, the SVM-PSO technique is used to determine the optimal power generation from each source and HVDC line restoration sequences for minimizing power loss and shedding load with system constraints. Table 8 presents several failure simulations on the system's lines and the SVM-PSO solutions to these failures. Also, from this table, it can be seen that, when the failure occurs in the HVDC line direct connecting power source to the load at bus 4, the power loss increases due to the power circulation from that source through the network until reach to supplying the load.

In general, the proposed protection scheme can detect and clear the faults that may occur in the MT-HVDC transmission grids in an acceptable time. Also, it preserves the steady-state operation after the fault clearance in a fast time. This work is based on time-sensitive networking using data distribution services. It synchronizes multiple devices using packet-based communication and makes it possible over long distances without any signal propagation delay. Input/output (I/O) synchronization on devices using this profile is less than 1 μs. It can be further reduced to the hundreds of nanoseconds range, depending on the system's configuration.

VII. CONCLUSION

This paper proposed a protection scheme for the MT-HVDC transmission grids. The proposed scheme is composed of three protection levels. After the disconnection of the MT-HVDC grid in the third level, the SVM has been proposed to discriminate the faulty line and then reconnect the healthy line in the MT-HVDC transmission grid. The healthy lines' restoration process is based on the PSO algorithm to obtain the optimal line restoration sequence to maximize the restored load and minimize the power loss while ensuring the operational constraints and the power balance. The fault tripping in the first two levels is based on the FIDs in the MT-HVDC grid. The communication between the AC grid and the HVDC grid is based on IoT technology. The proposed protection scheme has been applied and verified on a hypothetical MT-HVDC grid in the presence of different fault conditions. The results show the proposed protection scheme's ability to detect and clear the fault in good time. Also, the proposed protection preserves the steady-state operation as fast as possible. The following conclusion can be drawn;

- After the fault occurrence, the fault clearing time achieved with the proposed protection scheme is 1.22 ms, 2.22 ms, 3.22 ms with the main, backup one, and backup two protection levels respectively under different fault conditions. Also, the load steady state operating time preserved with the proposed scheme is 0.2 s, 0.25 s, 0.40 s with the main, backup one, and backup two protection levels respectively.
- The SVM classification method provides an overall training accuracy which obtained when trained over training data of about 98.6%. The testing accuracy that obtained when trained over testing data is about 99.2%.
- The proposed SVM based faulty line identification has an offline training time of 75 s and the faulty line is detected after 15 ms with 62.50 %

REFERENCES

[1] Q. Huang, G. Zou, X. Wei, C. Sun, and H. Gao, "A non-unit line protection scheme for MMC-based multi-terminal HVDC grid," *Int. J. Electr. Power Energy Syst.*, vol. 107, pp. 1–9, May 2019, doi: 10.1016/j.ijepes.2018.11.008.

[2] A. Raza, A. Akhtar, M. Jamil, G. Abbas, S. O. Gilani, L. Yuchao, M. N. Khan, T. Izhar, X. Dianguo, and B. W. Williams, "A protection scheme for multi-terminal VSC-HVDC transmission systems," *IEEE Access*, vol. 6, pp. 3159–3166, 2018, doi: 10.1109/ACCESS.2017.2787485.

[3] B. Li, J. He, Y. Li, and B. Li, "A review of the protection for the multi-terminal VSC-HVDC grid," *Protection Control Mod. Power Syst.*, vol. 4, no. 1, Dec. 2019, Art. no. 21, doi: 10.1186/s41601-019-0136-2.

[4] A. Meghwani, S. C. Srivastava, and S. Chakrabarti, "A non-unit protection scheme for DC microgrid based on local measurements," *IEEE Trans. Power Del.*, vol. 32, no. 1, pp. 172–181, Feb. 2017, doi: 10.1109/TPWRD.2016.2555844.

[5] A. R. Adly, S. H. E. A. Aleem, M. A. Algabalawy, F. Jurado, and Z. M. Ali, "A novel protection scheme for multi-terminal transmission lines based on wavelet transform," *Electr. Power Syst. Res.*, vol. 183, Jun. 2020, Art. no. 106286, doi: 10.1016/j.epsr.2020.106286.

[6] D. Tzelepis, A. Dysko, G. Fusiek, J. Nelson, P. Niewczas, D. Vozikis, P. Orr, N. Gordon, and C. D. Booth, "Single-ended differential protection in MTDC networks using optical sensors," *IEEE Trans. Power Del.*, vol. 32, no. 3, pp. 1605–1615, Jun. 2017, doi: 10.1109/TPWRD.2016.2645231.

[7] R. Ara, U. A. Khan, A. I. Bhatti, and B. W. Lee, "A reliable protection scheme for fast DC fault clearance in a VSC-based meshed MTDC grid," *IEEE Access*, vol. 8, pp. 88188–88199, 2020, doi: 10.1109/ACCESS.2020.2993001.

[8] J. Zheng, M. Wen, Y. Chen, and X. Shao, "A novel differential protection scheme for HVDC transmission lines," *Int. J. Electr. Power Energy Syst.*, vol. 94, pp. 171–178, Jan. 2018, doi: 10.1016/j.ijepes.2017.07.006.

[9] S. Zhang, G. Zou, C. Wang, J. Li, and B. Xu, "A non-unit boundary protection of DC line for MMC-MTDC grids," *Int. J. Electr. Power Energy Syst.*, vol. 116, Mar. 2020, Art. no. 105538, doi: 10.1016/j.ijepes.2019.105538.

[10] X. Chen, H. Li, Y. Liang, and G. Wang, "A protection scheme for hybrid multi-terminal HVDC networks utilizing a time-domain transient voltage based on fault-blocking converters," *Int. J. Electr. Power Energy Syst.*, vol. 118, Jun. 2020, Art. no. 105825, doi: 10.1016/j.ijepes.2020.105825.

[11] B. Li, Y. Li, J. He, B. Li, S. Liu, B. Liu, and L. Xu, "An improved transient traveling-wave based direction criterion for multi-terminal HVDC grid," *IEEE Trans. Power Del.*, vol. 35, no. 5, pp. 2517–2529, Oct. 2020, doi: 10.1109/TPWRD.2020.2971103.

[12] M. Hajian, L. Zhang, and D. Jovcic, "DC transmission grid with low-speed protection using mechanical DC circuit breakers," *IEEE Trans. Power Del.*, vol. 30, no. 3, pp. 1383–1391, Jun. 2015, doi: 10.1109/TPWRD.2014.2371618.

[13] J. Sneath and A. D. Rajapakse, "Fault detection and interruption in an earthed HVDC grid using ROCOV and hybrid DC breakers," *IEEE Trans. Power Del.*, vol. 31, no. 3, pp. 973–981, Jun. 2016, doi: 10.1109/TPWRD.2014.2364547.

[14] W. Wang, M. Barnes, O. Marjanovic, and O. Cwikowski, "Impact of DC breaker systems on multiterminal VSC-HVDC stability," *IEEE Trans. Power Del.*, vol. 31, no. 2, pp. 769–779, Apr. 2016, doi: 10.1109/TPWRD.2015.2409132.

[15] X. Feng, L. Qi, and J. Pan, "A novel fault location method and algorithm for DC distribution protection," *IEEE Trans. Ind. Appl.*, vol. 53, no. 3, pp. 1834–1840, May 2017, doi: 10.1109/TIA.2017.2666083.

[16] S. Jamali and S. S. Mirhosseini, "Protection of transmission lines in multi-terminal HVDC grids using travelling waves morphological gradient," *Int. J. Electr. Power Energy Syst.*, vol. 108, pp. 125–134, Jun. 2019, doi: 10.1016/j.ijepes.2019.01.012.

[17] M. Elgeziry, M. Elsadd, N. Elkalashy, T. Kawady, A. Taalab, and M. A. Izzularab, "Non-pilot protection scheme for multi-terminal VSC-HVDC transmission systems," *IET Renew. Power Gener.*, vol. 13, no. 16, pp. 3033–3042, Dec. 2019, doi: 10.1049/iet-rpg.2018.6265.

[18] Y. Zhang and W. Cong, "An improved single-ended frequency-domain-based fault detection scheme for MMC-HVDC transmission lines," *Int. J. Electr. Power Energy Syst.*, vol. 125, Feb. 2021, Art. no. 106463, doi: 10.1016/j.ijepes.2020.106463.

[19] Y. Zhang, W. Cong, G. Li, K. Sun, and Y. Zhang, "Single-ended MMC-MTDC line protection based on dual-frequency amplitude ratio of traveling wave," *Electr. Power Syst. Res.*, vol. 189, Dec. 2020, Art. no. 106808, doi: 10.1016/j.epsr.2020.106808.

[20] R. E. Torres-Olguin and H. K. Hoidalen, "Inverse time overcurrent protection scheme for fault location in multi-terminal HVDC," in *Proc. IEEE Eindhoven PowerTech*, Jun./Jul. 2015, pp. 1–6, doi: 10.1109/PTC.2015.7232673.

[21] S. P. Azad and D. Van Hertem, "A fast local bus current-based primary relaying algorithm for HVDC grids," *IEEE Trans. Power Del.*, vol. 32, no. 1, pp. 193–202, Feb. 2017, doi: 10.1109/TPWRD.2016.2595323.

[22] R. Li, L. Xu, and L. Yao, "DC fault detection and location in meshed multiterminal HVDC systems based on DC reactor voltage change rate," *IEEE Trans. Power Del.*, vol. 32, no. 3, pp. 1516–1526, Jun. 2017, doi: 10.1109/TPWRD.2016.2590501.

[23] K. De Kerf, K. Srivastava, M. Reza, D. Bekaert, S. Cole, D. Van Hertem, and R. Belmans, "Wavelet-based protection strategy for DC faults in multi-terminal VSC HVDC systems," *IET Gener., Transmiss. Distrib.*, vol. 5, no. 4, p. 496, 2011, doi: 10.1049/iet-gtd.2010.0587.

[24] G. Zou, Q. Feng, Q. Huang, C. Sun, and H. Gao, "A fast protection scheme for VSC based multi-terminal DC grid," *Int. J. Electr. Power Energy Syst.*, vol. 98, pp. 307–314, Jun. 2018, doi: 10.1016/j.ijepes.2017.12.022.

[25] B. Mitra, B. Chowdhury, and A. Willis, "Protection coordination for assembly HVDC breakers for HVDC multiterminal grids using wavelet transform," *IEEE Syst. J.*, vol. 14, no. 1, pp. 1069–1079, Mar. 2020, doi: 10.1109/JSYST.2019.2922645.

[26] W. Leterme, N. Ahmed, J. Beerten, L. Ängquist, D. Van Hertem, and S. Norrga, "A new HVDC grid test system for HVDC grid dynamics and protection studies in EMT-type software," in *IET Seminar Dig.*, no. 654, 2015, pp. 1–7, doi: 10.1049/cp.2015.0068.

[27] A. E. B. Abu-Elanien, "Protection of star connected multi-terminal HVDC systems with offshore wind farms," in *Proc. IEEE 12th Int. Conf. Compat., Power Electron. Power Eng.*, Apr. 2018, pp. 1–6, doi: 10.1109/CPE.2018.8372485.

[28] K. Zhu, W. K. Lee, and P. W. T. Pong, "Fault-line identification of HVDC transmission lines by frequency-spectrum correlation based on capacitive coupling and magnetic field sensing," *IEEE Trans. Magn.*, vol. 54, no. 11, pp. 1–5, Nov. 2018, doi: 10.1109/TMAG.2018.2830803.

[29] N. Tong, X. Lin, C. Li, Q. Sui, L. Chen, Z. Wang, N. Jin, and Z. Li, "Permissive pilot protection adaptive to DC fault interruption for VSC-MTDC," *Int. J. Electr. Power Energy Syst.*, vol. 123, Dec. 2020, Art. no. 106234, doi: 10.1016/j.ijepes.2020.106234.

[30] M. Monadi, C. Koch-Ciobotaru, A. Luna, J. I. Candela, and P. Rodriguez, "Multi-terminal medium voltage DC grids fault location and isolation," *IET Gener., Transmiss. Distrib.*, vol. 10, no. 14, pp. 3517–3528, Nov. 2016, doi: 10.1049/iet-gtd.2016.0183.

[31] A. E. B. Abu-Elanien, A. A. Elserougi, A. S. Abdel-Khalik, A. M. Massoud, and S. Ahmed, "A differential protection technique for multi-terminal HVDC," *Electr. Power Syst. Res.*, vol. 130, pp. 78–88, Jan. 2016, doi: 10.1016/j.epsr.2015.08.021.

[32] S. Azizi, S. Afsharnia, and M. Sanaye-Pasand, "Fault location on multi-terminal DC systems using synchronized current measurements," *Int. J. Electr. Power Energy Syst.*, vol. 63, pp. 779–786, Dec. 2014, doi: 10.1016/j.ijepes.2014.06.040.

[33] S. H. Nandipati, P. T. Babu, M. Chigurupati, and C. Vaithilingam, "Interface protection and energy management system for microgrid using Internet of Things," *Energy Procedia*, vol. 117, pp. 201–208, Jun. 2017, doi: 10.1016/j.egypro.2017.05.123.

[34] F. Bonavolonta, C. Caputi, A. Liccardo, and A. Teotino, "Protection of MV smart grid based on IoT technology," in *Proc. 2nd Workshop Metrol. Ind. IoT*, 2019, pp. 112–116, doi: 10.1109/METROI4.2019.8792881.

[35] F. Aminifar, S. Teimourzadeh, A. Shahsavari, M. Savaghebi, and M. S. Golsorkhi, "Machine learning for protection of distribution networks and power electronics-interfaced systems," *Electr. J.*, vol. 34, no. 1, Jan. 2021, Art. no. 106886, doi: 10.1016/j.tej.2020.106886.

[36] A. Majee and O. V. G. Swathika, "IoT based reconfiguration of microgrids through an automated central protection centre," in *Proc. Int. Conf. Power Embedded Drive Control (ICPEDC)*, Mar. 2017, pp. 93–97, doi: 10.1109/ICPEDC.2017.8081066.

[37] W. An, W. Fei, X. Li, T. Le, and Z. Pan, "Development of a smart low voltage circuit breaker with integrated protection and control functions based on wireless communications," in *Proc. IEEE 8th Int. Conf. Adv. Power Syst. Automat. Protection (APAP)*, Oct. 2019, pp. 257–262, doi: 10.1109/APAP47170.2019.9225030.

[38] N. Yousefnezhad, A. Malhi, and K. Främling, "Security in product lifecycle of IoT devices: A survey," *J. Netw. Comput. Appl.*, vol. 171, Dec. 2020, Art. no. 102779, doi: 10.1016/j.jnca.2020.102779.

[39] H. R. Baghaee, D. Mlakic, S. Nikolovski, and T. Dragicevic, "Support vector machine-based islanding and grid fault detection in active distribution networks," *IEEE J. Emerg. Sel. Topics Power Electron.*, vol. 8, no. 3, pp. 2385–2403, Sep. 2020, doi: 10.1109/JESTPE.2019.2916621.

[40] H. Wang, M.-J. Peng, J. Wesley Hines, G.-Y. Zheng, Y.-K. Liu, and B. R. Upadhyaya, "A hybrid fault diagnosis methodology with support vector machine and improved particle swarm optimization for nuclear power plants," *ISA Trans.*, vol. 95, pp. 358–371, Dec. 2019, doi: 10.1016/j.isatra.2019.05.016.

[41] Y. Wang, Y. Zhu, Q. Wang, Y. Tang, F. Duan, and Y. Yang, "Complex fault source identification method for high-voltage trip-offs of wind farms based on SU-MRMR and PSO-SVM," *IEEE Access*, vol. 8, pp. 130379–130391, 2020, doi: 10.1109/ACCESS.2020.3008211.

[42] S. J. Xiao, S. Lan, Y. B. Yuan, M. J. Chen, and T. Jin, "A line fault type detection method based on optimal sample training support vector machine in MMC-HVDC transmission system," in *Proc. IEEE 8th Int. Conf. Adv. Power Syst. Automat. Protection (APAP)*, Oct. 2019, pp. 1769–1773, doi: 10.1109/APAP47170.2019.9224886.

[43] N. Qu, J. Zuo, J. Chen, and Z. Li, "Series arc fault detection of indoor power distribution system based on LVQ-NN and PSO-SVM," *IEEE Access*, vol. 7, pp. 184020–184028, 2019, doi: 10.1109/ACCESS.2019.2960512.

[44] X. Zhang, P. Han, L. Xu, F. Zhang, Y. Wang, and L. Gao, "Research on bearing fault diagnosis of wind turbine gearbox based on 1DCNN-PSO-SVM," *IEEE Access*, vol. 8, pp. 192248–192258, 2020, doi: 10.1109/ACCESS.2020.3032719.

[45] J.-Y. Wu, S. Lan, S.-J. Xiao, and Y.-B. Yuan, "Single pole-to-ground fault location system for MMC-HVDC transmission lines based on active pulse and CEEMDAN," *IEEE Access*, vol. 9, pp. 42226–42235, 2021, doi: 10.1109/ACCESS.2021.3062703.

[46] R. Muzzammel and A. Raza, "A support vector machine learning-based protection technique for MT-HVDC systems," *Energies*, vol. 13, no. 24, p. 6668, Dec. 2020, doi: 10.3390/en13246668.
[47] A. K. Tamrakar and E. Koley, "A SVM based fault detection and section identification scheme for a hybrid AC/HVDC transmission line with wind farm integration," in *Proc. IEEE 1st Int. Conf. Smart Technol. Power, Energy Control (STPEC)*, Sep. 2020, pp. 1–5, doi: 10.1109/stpec49749.2020.9297720.
[48] P. W. T. Pong, A. M. Annaswamy, B. Kroposki, Y. Zhang, R. Rajagopal, G. Zussman, and H. V. Poor, "Cyber-enabled grids: Shaping future energy systems," *Adv. Appl. Energy*, vol. 1, Feb. 2021, Art. no. 100003, doi: 10.1016/j.adapen.2020.100003.
[49] M. El-Hajj, A. Fadlallah, M. Chamoun, and A. Serhrouchni, "A survey of Internet of Things (IoT) authentication schemes," *Sensors*, vol. 19, no. 5, p. 1141, Mar. 2019, doi: 10.3390/s19051141.
[50] L. Tightiz and H. Yang, "A comprehensive review on IoT protocols' features in smart grid communication," *Energies*, vol. 13, no. 11, p. 2762, Jun. 2020, doi: 10.3390/en13112762.
[51] N. H. Ali, B. M. Ali, M. L. Othman, and K. M. Abdel-Latif, "Performance of communication networks for integrity protection systems based on travelling wave with IEC 61850," *Int. J. Electr. Power Energy Syst.*, vol. 95, pp. 664–675, Feb. 2018, doi: 10.1016/j.ijepes.2017.09.024.
[52] A. Chandra, G. K. Singh, and V. Pant, "Protection techniques for DC microgrid—A review," *Electric Power Syst. Res.*, vol. 187, Oct. 2020, Art. no. 106439, doi: 10.1016/j.epsr.2020.106439.
[53] I. Jahn, F. Hohn, G. Chaffey, and S. Norrga, "An open-source protection IED for research and education in multiterminal HVDC grids," *IEEE Trans. Power Syst.*, vol. 35, no. 4, pp. 2949–2958, Jul. 2020, doi: 10.1109/TPWRS.2020.2970477.
[54] Y. Zhang, Y. Li, J. Song, X. Chen, Y. Lu, and W. Wang, "Pearson correlation coefficient of current derivatives based pilot protection scheme for long-distance LCC-HVDC transmission lines," *Int. J. Electr. Power Energy Syst.*, vol. 116, Mar. 2020, Art. no. 105526, doi: 10.1016/j.ijepes.2019.105526.
[55] M. Muniappan, "A comprehensive review of DC fault protection methods in HVDC transmission systems," *Protection Control Mod. Power Syst.*, vol. 6, no. 1, pp. 1–20, Dec. 2021, doi: 10.1186/s41601-020-00173-9.
[56] M. J. P. Molina, D. M. Larruskain, P. E. López, and A. Etxegarai, "Analysis of local measurement-based algorithms for fault detection in a multiterminal HVDC grid," *Energies*, vol. 12, no. 24, p. 4808, Dec. 2019, doi: 10.3390/en12244808.
[57] F. Tian, X. Zhou, Z. Yu, D. Shi, Y. Chen, and Y. Huang, "A preventive transient stability control method based on support vector machine," *Electric Power Syst. Res.*, vol. 170, pp. 286–293, May 2019, doi: 10.1016/j.epsr.2019.01.030.
[58] Y. Zhou, J. Wu, L. Ji, Z. Yu, K. Lin, and L. Hao, "Transient stability preventive control of power systems using chaotic particle swarm optimization combined with two-stage support vector machine," *Electr. Power Syst. Res.*, vol. 155, pp. 111–120, Feb. 2018, doi: 10.1016/j.epsr.2017.10.007.
[59] A. E. B. Abu-Elanien, A. S. Abdel-Khalik, A. M. Massoud, and S. Ahmed, "A non-communication based protection algorithm for multi-terminal HVDC grids," *Electr. Power Syst. Res.*, vol. 144, pp. 41–51, Mar. 2017, doi: 10.1016/j.epsr.2016.11.010.
[60] S. Beheshtaein, R. M. Cuzner, M. Forouzesh, M. Savaghebi, and J. M. Guerrero, "DC microgrid protection: A comprehensive review," *IEEE J. Emerg. Sel. Topics Power Electron.*, early access, Mar. 12, 2019, doi: 10.1109/jestpe.2019.2904588.
[61] G. Song, T. Wang, and K. S. T. Hussain, "DC line fault identification based on pulse injection from hybrid HVDC breaker," *IEEE Trans. Power Del.*, vol. 34, no. 1, pp. 271–280, Feb. 2019, doi: 10.1109/TPWRD.2018.2865226.
[62] H. Noura, T. Hatoum, O. Salman, J.-P. Yaacoub, and A. Chehab, "LoRaWAN security survey: Issues, threats and possible mitigation techniques," *Internet Things*, vol. 12, Dec. 2020, Art. no. 100303, doi: 10.1016/j.iot.2020.100303.
[63] J. Klomjit and A. Ngaopitakkul, "Comparison of artificial intelligence methods for fault classification of the 115-kV hybrid transmission system," *Appl. Sci.*, vol. 10, no. 11, p. 3967, Jun. 2020, doi: 10.3390/app10113967.
[64] D. Mlakic, H. R. Baghaee, and S. Nikolovski, "A novel ANFIS-based islanding detection for inverter-interfaced microgrids," *IEEE Trans. Smart Grid*, vol. 10, no. 4, pp. 4411–4424, Jul. 2019, doi: 10.1109/TSG.2018.2859360.

ABDELFATTAH A. ELADL received the B.Sc. (Hons.), M.Sc., and Ph.D. degrees in electrical engineering from the Faculty of Engineering-Mansoura University, EL-Mansoura, Egypt. He is currently an Associate Professor with the Electrical Engineering Department, Mansoura University. His research interests include power system economics, planning, power quality, protection, and energy hubs. In 2016, he received the Best Ph.D. Thesis Award from Mansoura University.

MOHAMMED A. SAEED received the B.Sc. degree, in 2004, and the M.S. and Ph.D. degrees in electrical power and machines engineering from Mansoura University, Egypt, in 2010 and 2015, respectively. In 2005, he joined as a Temporary Researcher with the Department of Electrical Engineering, Mansoura University, where he has been received a permanent position as an Assistant Professor, since 2015. He travelled as a Visiting Scholar to South Africa, USA, and Poland for different scientific missions for different durations from Erasmus+ and Fulbright programs. His research interests include renewable energy, biomass energy, smart grids, advanced control, modern optimization techniques, and power system analysis.

BISHOY E. SEDHOM (Member, IEEE) received the B.Sc. (Hons.), M.Sc., and Ph.D. degrees in electrical engineering from the Faculty of Engineering-Mansoura University, EL-Mansoura, Egypt. He is currently an Assistant Professor with the Electrical Engineering Department, Mansoura University. His research interests include energy management, microgrid operation and control, power system protection, power quality, the Internet of Things, optimization methods, islanding detection, and system restoration. In 2019, he received the Best Ph.D. Thesis Award from Mansoura University.

JOSEP M. GUERRERO (Fellow, IEEE) received the B.S. degree in telecommunications engineering, the M.S. degree in electronics engineering, and the Ph.D. degree in power electronics from the Technical University of Catalonia, Barcelona, in 1997, 2000, and 2003, respectively. Since 2011, he has been a Full Professor with the Department of Energy Technology, Aalborg University, Denmark, where he is responsible for the Microgrid Research Program. Since 2014, he has been the Chair Professor with Shandong University. Since 2015, he has been a Distinguished Guest Professor with Hunan University. Since 2016, he has been a Visiting Professor Fellow with Aston University, U.K., and a Guest Professor with the Nanjing University of Posts and Telecommunications. In 2019, he became a Villum Investigator with the Villum Fonden, which supports the Center for Research on Microgrids (CROM), Aalborg University, where he is the Founder and the Director. He has published more than 500 journal articles in the fields of microgrids and renewable energy systems, which are cited more than 50 000 times. His research interests include different microgrid aspects, including power electronics, distributed energy-storage systems, hierarchical and cooperative control, energy management systems, smart metering, and the Internet of Things for ac/dc microgrid clusters and islanded minigrids, with a special focus on microgrid technologies applied to offshore wind and maritime microgrids for electrical ships, vessels, ferries, and seaports. He received the Best Paper Award of the IEEE TRANSACTIONS ON ENERGY CONVERSION, from 2014 to 2015, the Best Paper Prize of IEEE-PES, in 2015, and the Best Paper Award of the IEEE OPEN JOURNAL OF POWER ELECTRONICS, in 2016. From 2014 to 2019, he was awarded by the Clarivate Analytics (former Thomson Reuters) as a Highly Cited Researcher. He is an Associate Editor of a number of IEEE TRANSACTIONS.